

Article

Analysis of Cooling Characteristics of Permanent Magnet Synchronous Motor with Different Water Jacket Design Using Electromagnetic–Thermal Fluid Coupled Analysis and Design of Experiment

Kyunghun Jeon ¹, Myungwoo Park ¹, Jongjin Park ¹, Hongjun Choi ¹, Ki-Deok Lee ² , Jeong-Jong Lee ² and Chang-Wan Kim ^{3,*} 

¹ Graduate School of Mechanical Design & Production Engineering, Konkuk University, Seoul 05029, Republic of Korea

² Intelligent Mechatronics Research Center, Korea Electronics Technology Institute, Seongnam-si 13509, Republic of Korea

³ School of Mechanical Engineering, Konkuk University, Seoul 05029, Republic of Korea

* Correspondence: goodant@konkuk.ac.kr

Abstract: Electrical losses are converted into thermal energy in motors, which heats each component. It is a significant factor in decreasing motor mechanical performance. In this paper, the motor cooling characteristics were analyzed according to the design factors of the water jacket to investigate the cooling performance of a permanent magnet synchronous motor (PMSM). First, the electrical losses generated in PMSM were calculated using electromagnetic finite element (FE) analysis. Secondly, a 3D electromagnetic–thermal fluid coupled FE analysis was performed to analyze the temperature distribution inside the motor by applying electrical loss as the heat source. Finally, the motor cooling performance according to the design factors of the water jacket was statistically analyzed using the design of experiment (DOE) method. It was found that the mass flow rate of 0.02547 kg/s and six passes of the water jacket with one inlet and two outlets could be considered the optimum conditions in terms of the maximum motor temperature.

Keywords: Permanent Magnet Synchronous Motor (PMSM); cooling; electrical losses; water jacket; electromagnetic–thermal fluid coupled analysis; Design Of Experiment (DOE); design factor analysis



Citation: Jeon, K.; Park, M.; Park, J.; Choi, H.; Lee, K.-D.; Lee, J.-J.; Kim, C.-W. Analysis of Cooling Characteristics of Permanent Magnet Synchronous Motor with Different Water Jacket Design Using Electromagnetic–Thermal Fluid Coupled Analysis and Design of Experiment. *Machines* **2023**, *11*, 903. <https://doi.org/10.3390/machines11090903>

Academic Editor: Giacomo Scelba

Received: 30 July 2023

Revised: 28 August 2023

Accepted: 8 September 2023

Published: 11 September 2023



Copyright: © 2023 by the authors. Licensee MDPI, Basel, Switzerland. This article is an open access article distributed under the terms and conditions of the Creative Commons Attribution (CC BY) license (<https://creativecommons.org/licenses/by/4.0/>).

1. Introduction

Recently, fuel efficiency regulations for internal combustion engine vehicles have been strengthened, and the number of electric vehicles has proliferated. Accordingly, the motor, which serves as the propulsion source for electric vehicles, needs to have significant power. To increase the power of the motor, a substantial current is required in the motor windings. As the current increases, the electrical loss increases, and the electrical loss becomes a heat source for the motor [1]. When the temperature of the insulation part exceeds the allowable temperature due to the heat generated inside the motor, the insulation performance decreases, which may cause a motor burnout problem. In addition, when the temperature of the permanent magnet exceeds the limiting temperature for irreversible demagnetization, its performance and motor power may decrease [2,3]. Therefore, studies have been actively conducted to analyze motors' internal temperature [4–6].

Jiang et al. [4] proposed a method to predict a motor's internal temperature and electromagnetic performance according to temperature through electromagnetic–thermal coupled analysis. Boglietti et al. [5] proposed a method to calculate the equivalent thermal conductivity of a winding insulation system, which is one of the main issues in the thermal modeling of electric motors. Li et al. [6] analyzed the effect of the thermal conductivity of

motor alloys on motor temperature distribution using electromagnetic–thermal coupled analysis.

Mi et al. [7] evaluated the temperature of a permanent magnet synchronous motor due to iron loss using the finite element method. Inamura et al. [8] analyzed the increase in the switched reluctance motor's temperature due to copper and core loss. Although these studies effectively analyze the internal temperature distribution of the motor, it is difficult to apply them to lower the motor's internal temperature directly. Therefore, studies to lower the internal temperature of motors have been actively conducted [9–11].

Chen et al. [9] optimized the stator shaft diameter and the position of the rotor axial vent holes to lower the motor's internal temperature. Cavazzut et al. [10] analyzed the main parameters affecting the motor winding temperature and optimized the stator geometries. Lim et al. [11] optimized the rotor shape to improve the torque performance of interior permanent magnet motors by considering the thermal properties of permanent magnets. However, assuming the shape of the stator and the rotor changes, the motor's internal resistance will change, and thus the electromagnetic characteristics of the motor will change [12]. In contrast, motor housing addresses this problem and has sufficient space to construct a water jacket. Therefore, studies have been conducted to analyze the characteristics of the motor housing water jacket and lower the internal temperature of the motor [13–16].

Zhang et al. [13] analyzed the motor cooling performance by considering the number of water jacket passes, width, and height as design variables. Ye et al. [14] analyzed the cooling characteristics of the motor according to the type of water jacket. Lee et al. [15] analyzed the maximum motor temperature using the water jacket path. Liang et al. [16] analyzed the maximum motor temperature according to the water jacket's width, length, and thermal conductivity. When the distribution of the flow rate inside the cooling water channel is uniform, the location and number of inlets/outlets of the cooling water channel can be considered as parameters that affect the cooling performance, such as the maximum temperature and pressure drop of the motor. Therefore, in order to improve the cooling performance, it is necessary to analyze the effect of the location and number of inlets and outlets of cooling water on the cooling performance. Previous studies have focused on the effect of cooling characteristics of the motor according to the mass flow rate, the number of water jacket passes, and thermal conductivity. There are few studies on the analysis of the cooling performance of the motor considering the location as well as the number of inlets and outlets of the water jacket.

In this paper, the cooling characteristics of the PMSM were statistically analyzed using the design of experiment (DOE) method with different numbers of water jacket passes, mass flow rates, and locations, as well as different numbers of inlets and outlets. The electromagnetic FE analysis was used to calculate the copper loss of the windings, the hysteresis loss of the stator, and the eddy-current loss of the permanent magnet at the maximum current and rated rotation speed of the motor. The electromagnetic–thermal fluid coupled analysis was performed using each component's calculated electrical loss as the heat source. The thermal fluid FE model consisted of a full 3D model, including the end winding. The cooling characteristics according to the design parameters were analyzed by considering the motor's maximum temperature and pressure drop using DOE.

2. Electrical Loss Calculations with Electromagnetic Finite Element Analysis

A 2D electromagnetic analysis was performed for a four-pole 24-slot PMSM, as shown in Figure 1. The FE model for electromagnetic analysis consists of a stator core, rotor core, permanent magnet, winding, air gap, and shaft, which is shown in Figure 2. The specifications of the motor and the material properties of each component are listed in Tables 1 and 2, respectively. Thermal conductivity values are commonly considered constant, and the magnetic permeability that changes according to the magnetization force is applied to silicon, which is the material of the stator and rotor, and the B–H curve of silicon is shown in Figure 3. Electromagnetic analysis was solved using Altair flux [17].

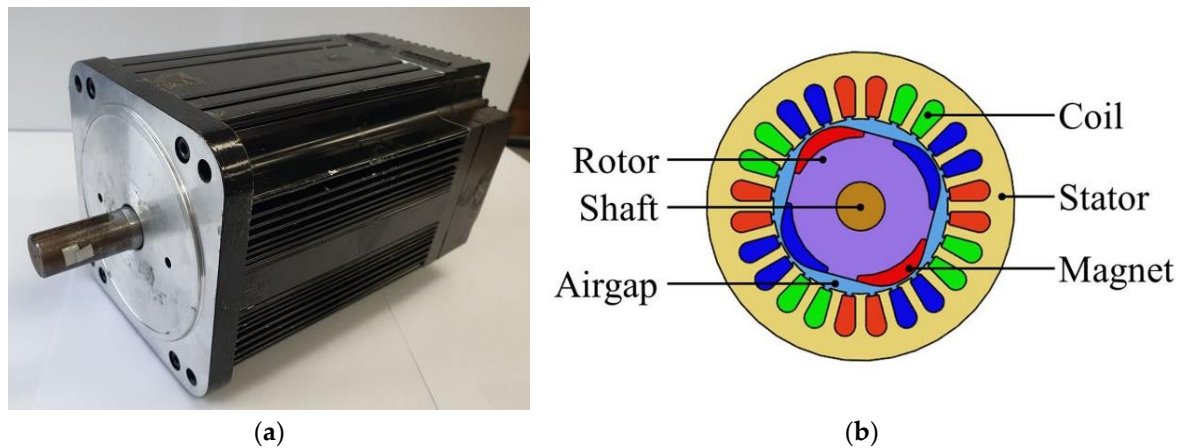


Figure 1. Permanent magnet synchronous motor (PMSM): (a) motor configuration; (b) cross-section.

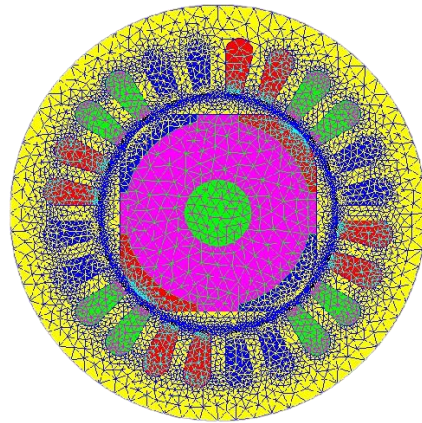


Figure 2. Finite element model of PMSM.

Table 1. PMSM specifications.

Specification	Quantity
Type of permanent magnet	Surface mount
Stator outer diameter	120 mm
Number of poles	4
Number of slots	24
Max. current	41 A
Rated voltage	48 V
Rated speed	2000 rpm
Rated power	1500 W

Table 2. Material properties.

Part (Material)	Residual Flux Density (T)	Permeability	Resistivity ($\Omega \cdot m$)	Thermal Conductivity (W/m·K)
Winding (copper)		1	1.7×10^{-8}	372.1
Magnet (N35SH)	1.2	1.05	14.9×10^{-8}	8.9
Shaft (steel)		30	6.25×10^{-7}	72.1
Rotor core		B-H curve (Figure 3)		
Stator core (silicon)			1.0×10^{12}	83.7

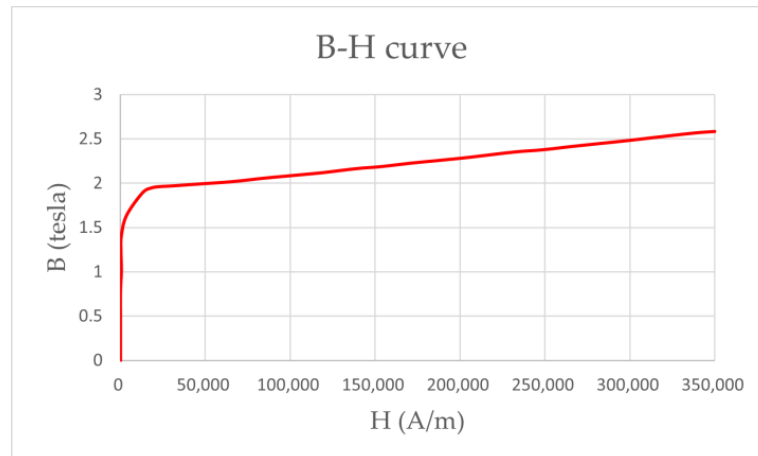


Figure 3. B–H curve of silicon.

The typical electrical losses that generate heat inside the PMSM are the copper loss of the winding, the iron loss of the stator, and the eddy-current loss of the permanent magnet. The copper loss occurs when electrical energy is converted into thermal energy due to the resistance of the winding, and it is calculated according to Equation (1) [8].

$$P_{copper} = J^2 \cdot \rho_{cu} \text{ [W / m}^3\text{]} \quad (1)$$

where P_{copper} is the copper loss density, J is the current density, and ρ_{cu} is the specific resistance of the winding. Meanwhile, the iron loss is caused by a change in the magnetic flux of a magnetic body. It is generally classified into hysteresis and eddy-current loss. The hysteresis loss occurs when the magnetic flux linking to the iron core alternately changes to the N and S poles and is calculated according to Equation (2).

$$P_h = K_h f B_{max}^n \text{ [W / m}^3\text{]} \quad (2)$$

where P_h is the hysteresis loss density, K_h is the hysteresis constant, f is the power supply frequency, B_{max} is the maximum magnetic flux density, and n is an experimental constant depending on the material, generally having a value of 1.5–2.5. Finally, the eddy-current loss refers to the loss due to the current in an eddy form caused by electromagnetic induction when the magnetic flux penetrates the iron core. It is calculated according to Equation (3).

$$P_e = k(tfB_{max})^2 \text{ [W / m}^3\text{]} \quad (3)$$

where P_e is the eddy-current loss density, k is the conductivity, and t is the thickness of the conductor passing through. The iron loss is expressed as the sum of hysteresis and eddy-current losses, which can be expressed as Equation (4) [7].

$$P_{iron} = P_h + P_e = K_h f B_{max}^n + k(tfB_{max})^2 \quad (4)$$

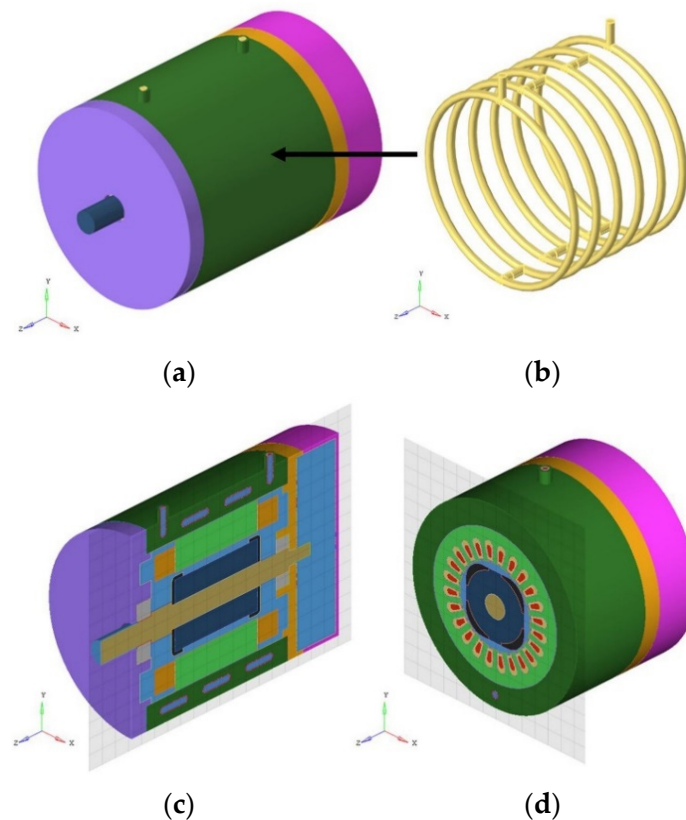
The motor loss calculated through 2D electromagnetic analysis was used as the motor's heat source. A three-phase current of up to 41 A was applied at a rotational speed of 2000 rpm, and copper loss, iron loss, and eddy-current loss occurred in the winding, stator, and permanent magnet of the PMSM, respectively. The calculated losses are shown in Table 3. Copper and hysteresis losses were dominant as they accounted for 99.3% of the electrical losses of the PMSM. The eddy-current loss was negligibly small. Therefore, only copper and hysteresis losses were considered, and the eddy-current loss was not considered a heat source for the electromagnetic–thermal fluid coupled analysis.

Table 3. Electric losses of the PMSM with FEM.

Copper	850 W
Hysteresis	51.5 W
Eddy current	6.26 W

3. Electromagnetic–Thermal Fluid Coupled FE Model of PMSM

Referring to the PMSM experiment presented in Figure 4, electromagnetic–thermal fluid coupled analysis was performed. Figure 5 shows the geometry of the motor and the shape of the water jacket inserted inside the housing, which was implemented to maintain the constant shapes of the stator and rotor. A water jacket in which the inlet and outlet exist one at each end was selected as the fundamental model.

**Figure 4.** Experiment of permanent magnet synchronous motor (PMSM) cooling system [18].**Figure 5.** A 3D geometrical model of the PMSM: (a) geometry of PMSM; (b) geometry of water jacket; (c) Y-Z plane cross-section of PMSM; (d) X-Y plane cross-section of PMSM.

The hysteresis loss, copper loss, and eddy-current loss calculated using the 2D electromagnetic FE analysis were divided by the stator, winding, and magnet volumes, respectively, to calculate the heat dissipation per unit volume. The electromagnetic–thermal fluid coupled analysis was performed using Acusolve. The inlet temperature of the cooling water was 303 K, and the outlet pressure was 0 Pa. A natural convection boundary condition, with a convection coefficient of $5 \text{ W/m}^2\cdot\text{K}$ and an ambient temperature of 298 K, was considered in the outer surface of the motor. In the air gap between the stator and the rotor, only conduction was considered.

The effect of the number of water jacket passes was analyzed using the electromagnetic–thermal fluid coupled analysis. In addition, the effects of design factors, such as the mass flow rate and location, as well as the number of inlets/outlets, on the cooling performance were analyzed. The mass flow rates of 0.00283–0.09339 kg/s were divided into five cases and applied to the inlet of the water jacket. Five representative cases of the water jacket were selected and analyzed, which are shown in Figure 6.

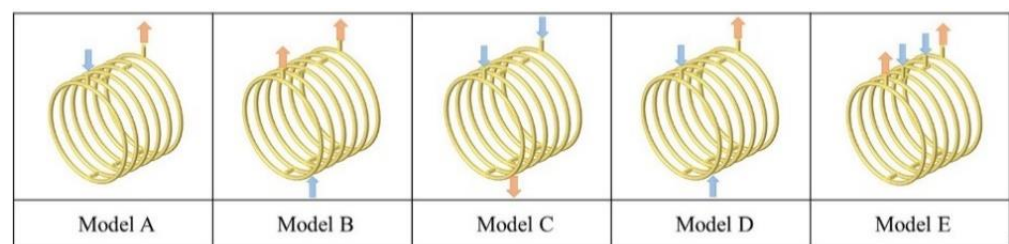


Figure 6. The geometry of the water jacket with different locations as well as numbers of inlets/outlets.

4. Analysis of Cooling Performance of Water Jacket with Design of Experiment (DOE)

To analyze the cooling performance according to the various design parameters, 25 cases of electromagnetic–thermal fluid coupled analysis were performed, as summarized in Table 4. The number of passes in the water jacket was determined to be six by analyzing the maximum motor temperature and pressure drop. The full factorial design method was used to investigate the effect of the mass flow rate and location, as well as the number of inlets/outlets, on the cooling characteristics of the housing water jacket. Considering that all factors consisted of five levels, 25 analyses were performed. The effect of each factor was analyzed through single-factor analysis, and for this, the maximum temperature and pressure drop inside the PMSM were analyzed as dependent variables.

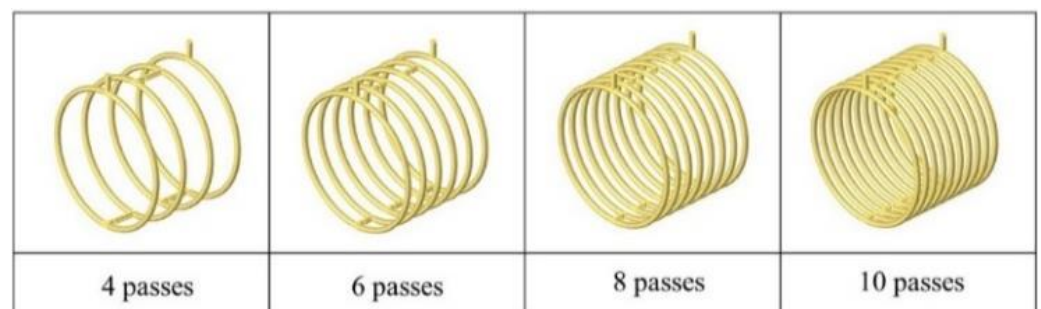
4.1. Effect of the Number of Water Jacket Passes

In order to determine the number of water jacket passes, the change in the maximum temperature of the motor and pressure drop were analyzed according to the number of water jacket passes. The investigated number of water jacket passes included 4, 6, 8, and 10, as illustrated in Figure 7. Figure 8a shows that the maximum motor temperature decreases when the number of passes increases. As the number of passes increases, the heat exchange area increases, so the maximum temperature inside the motor decreases. However, as the surface area of the water jacket increases, the frictional area also increases, and the flow velocity decreases. Therefore, the cooling performance does not increase beyond a specified number of passes. At a mass flow rate of 0.0283 kg/s, the maximum motor temperature decreases by 2.8 K when the number of passes increases from four to six. When it increases from 6 to 8 passes and from 8 to 10 passes, the maximum temperature decreases are 0.7 K and 0.3 K, respectively. The analytical results show no significant change in the cooling performance after six passes. The same trend is observed for all cases of mass flow rates. Figure 8b shows the change in pressure drop according to the number of water jacket passes. As the number of passes increases, the water jacket area increases, leading to more significant frictional losses.

Table 4. Electromagnetic–thermal fluid coupled analysis cases using DOE.

Case	Number of Passes	Inlet/Outlet Design	Mass Flow (kg/s)
1	6	Model A	0.00283
2			0.02547
3			0.04811
4			0.07075
5			0.09339
6		Model B	0.00283
7			0.02547
8			0.04811
9			0.07075
10			0.09339
11		Model C	0.00283
12			0.02547
13			0.04811
14			0.07075
15			0.09339
16		Model D	0.00283
17			0.02547
18			0.04811
19			0.07075
20			0.09339
21		Model E	0.00283
22			0.02547
23			0.04811
24			0.07075
25			0.09339

Consequently, the analysis reveals a trade-off between the maximum motor temperature and the pressure drop within the water jacket, depending on the number of passes. However, for more than six passes, the maximum temperature changes negligibly compared with the continuous increase in the pressure drop. Thus, the number of passes can be selected.

**Figure 7.** Water jacket geometries with different numbers of passes.

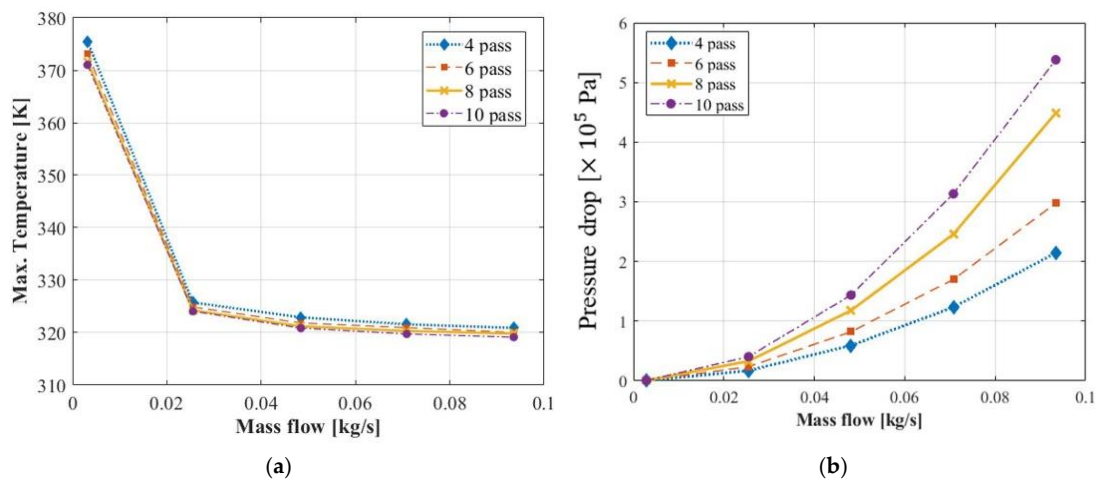


Figure 8. Maximum temperature and pressure drop with different number of passes and mass flow rates: (a) maximum temperature and (b) pressure drop.

4.2. Effect of Mass Flow Rate on Cooling Performance

In a water jacket with a uniform cross-sectional area, the convective heat transfer coefficient tends to increase as the mass flow rate of the coolant increases, resulting in a decrease in motor temperature and heat flux. Figures 9–11 show the distribution of motor temperature, pressure drop, and heat flux according to the mass flow rate when six passes of the water jacket are used. The motor’s maximum temperature and heat flux decrease as the mass flow rate increases. Figure 12a shows the maximum temperature of the motor as the mass flow rate increases from 0.00258 to 0.09339 kg/s. While the mass flow rate increases, the maximum temperature of the motor decreases sequentially by about 13%, 0.8%, 0.3%, and 0.2% at each interval. When the mass flow rate is higher than 0.02547 kg/s, it can be confirmed that the increase in mass flow rate has little effect on the decrease in the maximum temperature of the motor. Figure 12b shows the pressure drop of the water jacket according to the mass flow rate. As the mass flow rate increases, the pressure drop increases. This indicates a trade-off relationship with maximum temperature. However, when the mass flow rate exceeds 0.02547 kg/s, there is no significant difference in the maximum temperature of the motor compared with the exponential increase in pressure drop. Thus, an appropriate mass flow rate can be selected through this analysis.

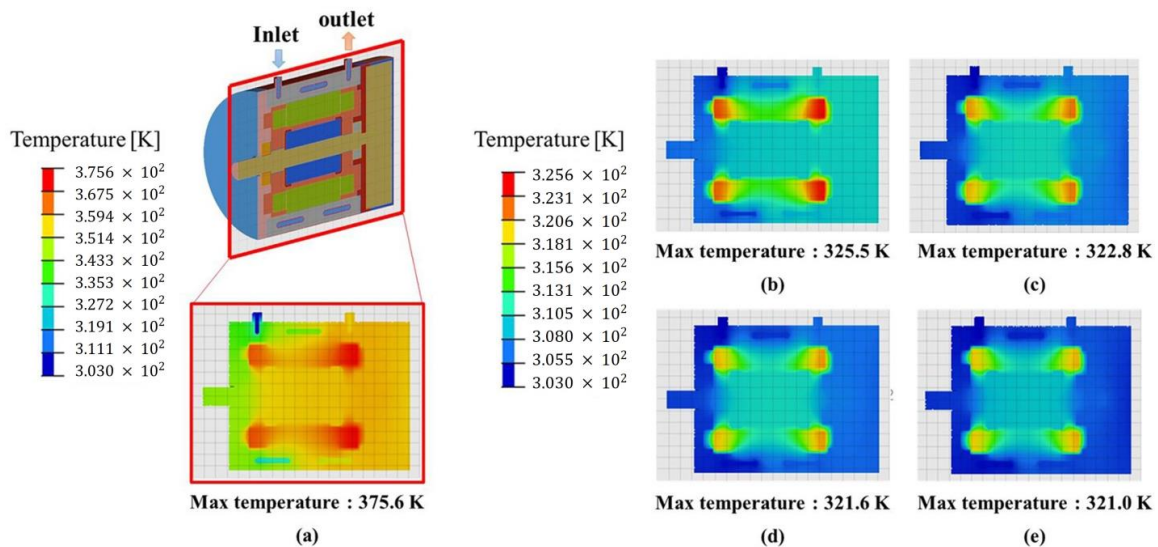


Figure 9. Temperature distribution of PMSM with water jacket of 6 passes with different mass flow rates: (a) 0.00283 kg/s; (b) 0.02547 kg/s; (c) 0.04811 kg/s; (d) 0.07075 kg/s; (e) 0.09339 kg/s.

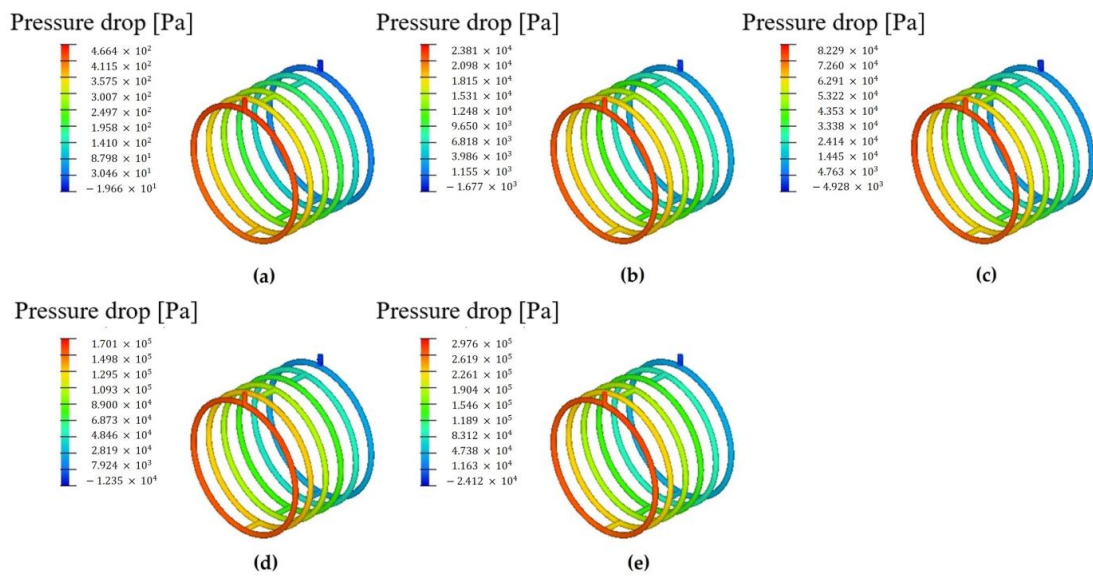


Figure 10. Pressure drop distribution of PMSM with water jacket of 6 passes with different mass flow rates: (a) 0.00283 kg/s; (b) 0.02547 kg/s; (c) 0.04811 kg/s; (d) 0.07075 kg/s; (e) 0.09339 kg/s.

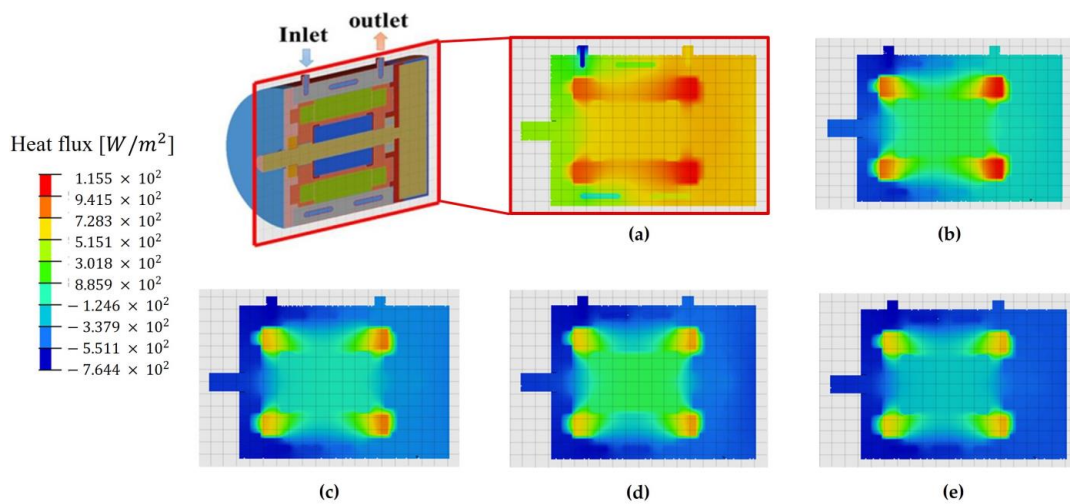


Figure 11. Heat flux distribution of PMSM with water jacket of 6 passes with different mass flow rates: (a) 0.00283 kg/s; (b) 0.02547 kg/s; (c) 0.04811 kg/s; (d) 0.07075 kg/s; (e) 0.09339 kg/s.

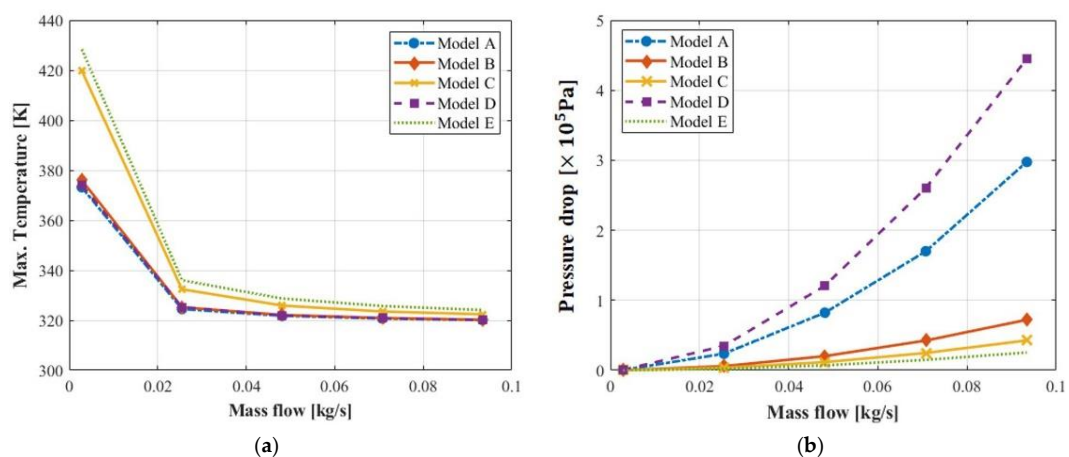


Figure 12. Maximum temperature and pressure drop with different locations and numbers of inlets/outlets and mass flow rates: (a) maximum temperature and (b) pressure drop.

4.3. Effect of the Location and Number of Inlets/Outlets on Cooling Performance

Considering the shape of the water jacket, five models with different locations and numbers of inlet/outlet were selected, as shown in Figure 6. In the case of Models C, D, and E, which had two inlets, the mass flow rate was equally distributed to each inlet. Figures 13–15 show the motor temperature, pressure drop, and heat flux distribution of the motor when the mass flow rate is 0.04811 kg/s. Maximum temperature and maximum heat flux occur in the end windings of the motor. Figure 12 shows the results of the electromagnetic–thermal fluid coupled analysis according to the location and number of inlets/outlets of the water jacket. Figure 12a shows the maximum temperature of the motor with the mass flow rate for each model according to the location and number of inlets/outlets. In the case of Model E, the mass flow through the path between the two inlets is small, so the motor temperature is the highest. Figure 16 shows the distribution of heat transfer coefficients on the surface of the water jacket. Model E has the lowest mean heat transfer coefficient. Thus, a small flow can be confirmed between the two inlets. In the case of Model C, by applying half the mass flow rate to the two inlets, the flow rate is reduced, the heat transfer performance deteriorates, and the maximum temperature inside the motor becomes the second highest. This is also confirmed considering the average value of the surface heat transfer coefficient of the water jacket in Figure 10. In the case of Model D, half the flow rate was applied to the two inlets, but after the middle of the water jacket, the two flow rates were combined. The heat transfer performance was relatively high. Model A shows the highest cooling performance for all other mass flow rate cases. However, the maximum temperature difference between Models A, B, and D is only 0.8%, which suggests the same cooling performance. Figure 12b shows the pressure drop in the water jacket with the mass flow rate for each model according to the location and number of inlets/outlets. In Model D, while the coolant flows, it merges with the coolant coming from another inlet, and the pressure rises. Therefore, a significant pressure drop occurs compared with the pressure drop observed in other models. Model A has one inlet and one outlet, and it has the longest path of water jacket compared with other models. Thus, more frictional losses occur, resulting in the second-largest pressure drop. Considering Figure 12 in the current motor, it is confirmed the pressure drop is small, and the maximum motor temperature is lowest in the case of Model B.

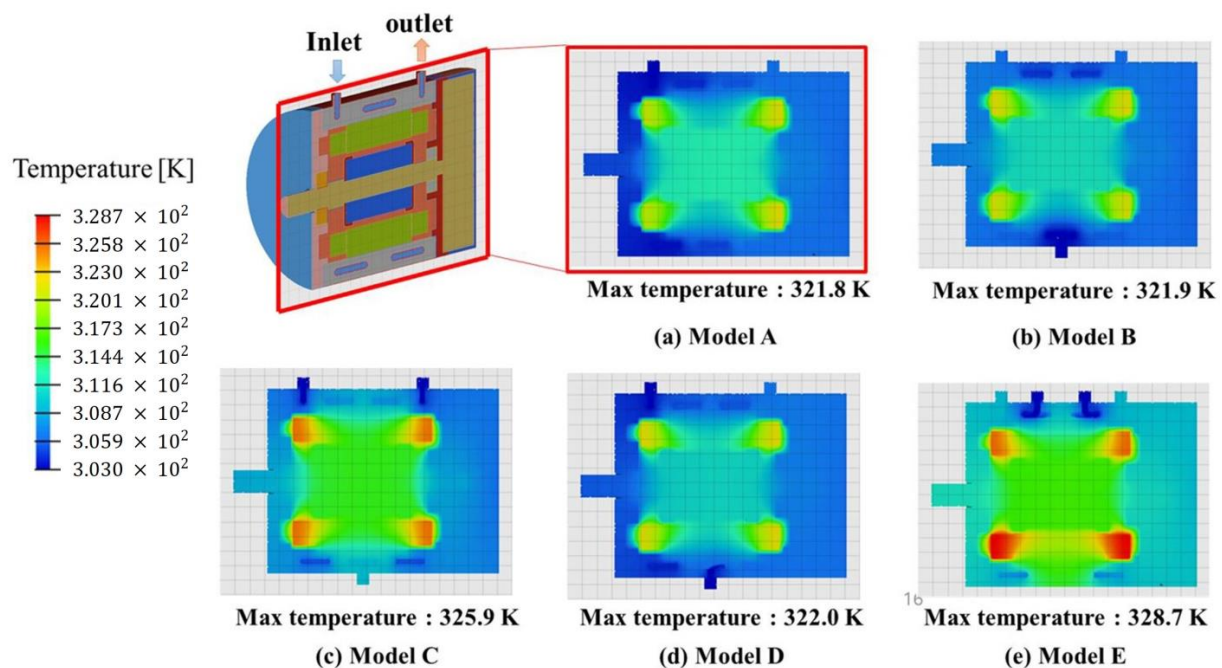


Figure 13. Temperature distribution of PMSM with different locations and numbers of inlets/outlets at the mass flow rate of 0.04811 kg/s.

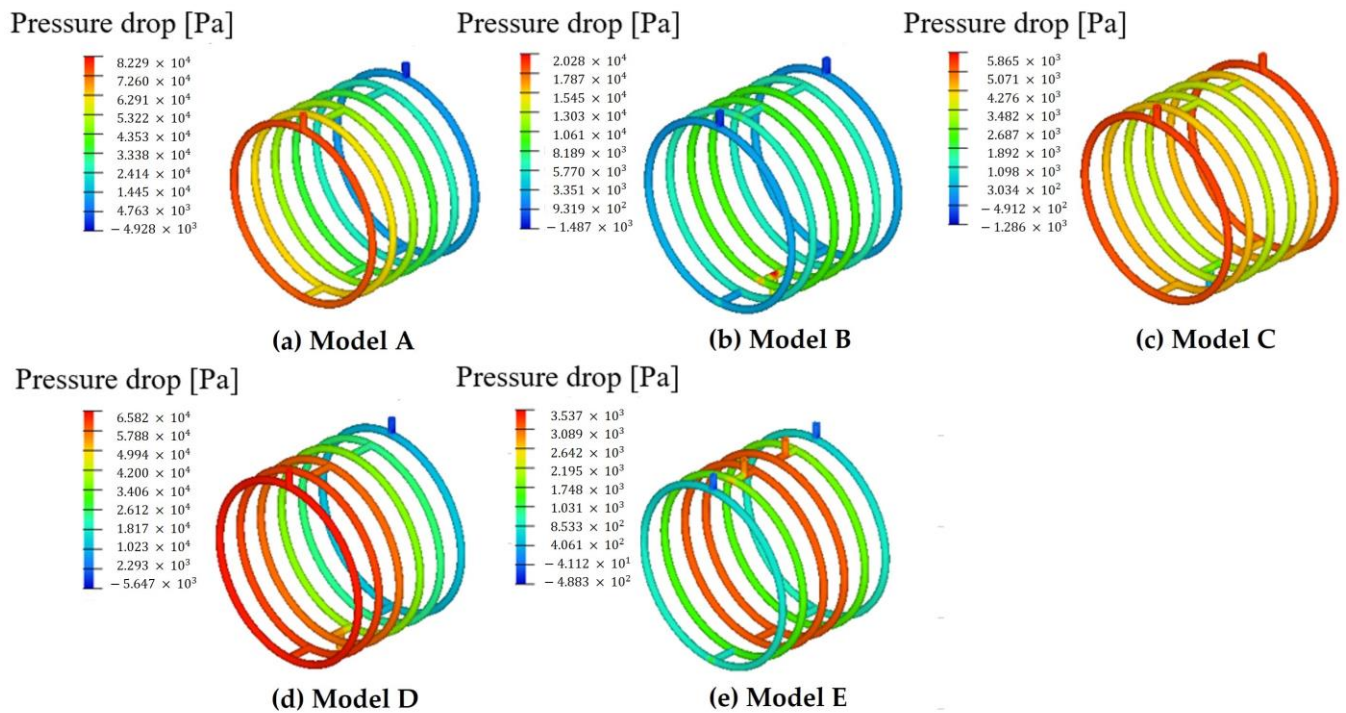


Figure 14. Pressure drop distribution of PMSM with different locations and numbers of inlets/outlets at the mass flow rate of 0.04811 kg/s.

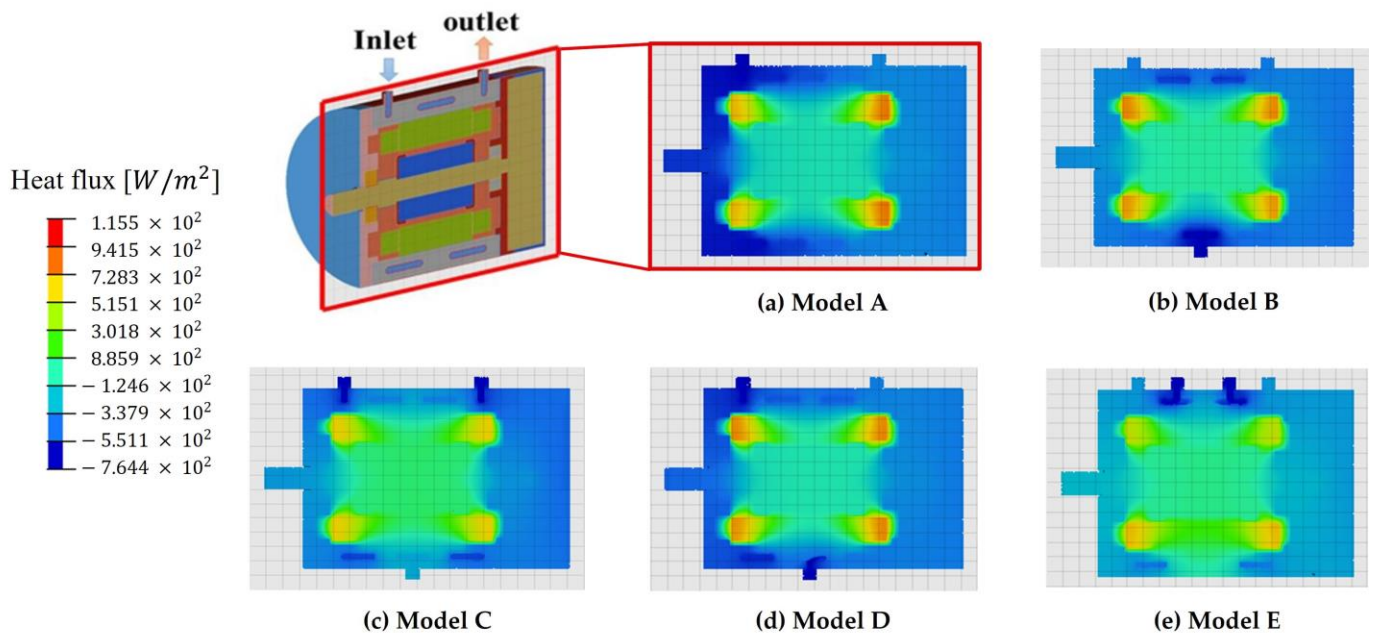


Figure 15. Heat flux distribution of PMSM with different locations and numbers of inlets/outlets at the mass flow rate of 0.04811 kg/s.

4.4. ANOVA (Analysis of Variance) for Temperature Difference and Pressure Drop

The effects of mass flow rate and the water jacket’s location and number of inlets/outlets were analyzed using ANOVA [19,20]. Figures 17 and 18 show the effect of the mass flow rate, the water jacket’s location, and the number of inlets/outlets on the maximum motor temperature and pressure drop. Figure 17 shows that the mass flow rate is the most effective design factor for the maximum motor temperature. The convective heat transfer coefficient, calculated using mass flow, determines the maximum motor temperature. Unlike the mass flow rate, the water jacket’s location and number of inlets/outlets

have little effect on the convective heat transfer coefficient, which determines the maximum motor temperature. Hence, the water jacket’s location and number of inlets/outlets are ineffective design factors for altering the maximum motor temperature. Figure 18 shows that the mass flow rate is the most important design factor for pressure drop. This is because the mass flow rate is directly used to calculate the pressure drop. In addition, it can be seen that the location and number of inlets/outlets of the water jacket are effective design factors for pressure drop. This means that the location and number of inlet/outlets of the water jacket affect the mass flow rate.

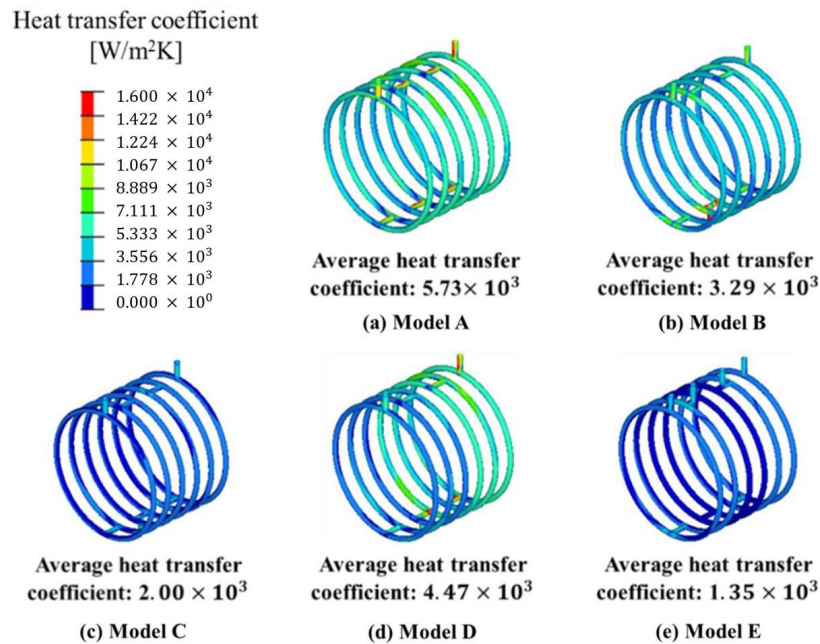


Figure 16. Heat transfer coefficient distribution on the water jacket surface with different locations and numbers of inlets/outlets at the mass flow rate of 0.02547 kg/s.

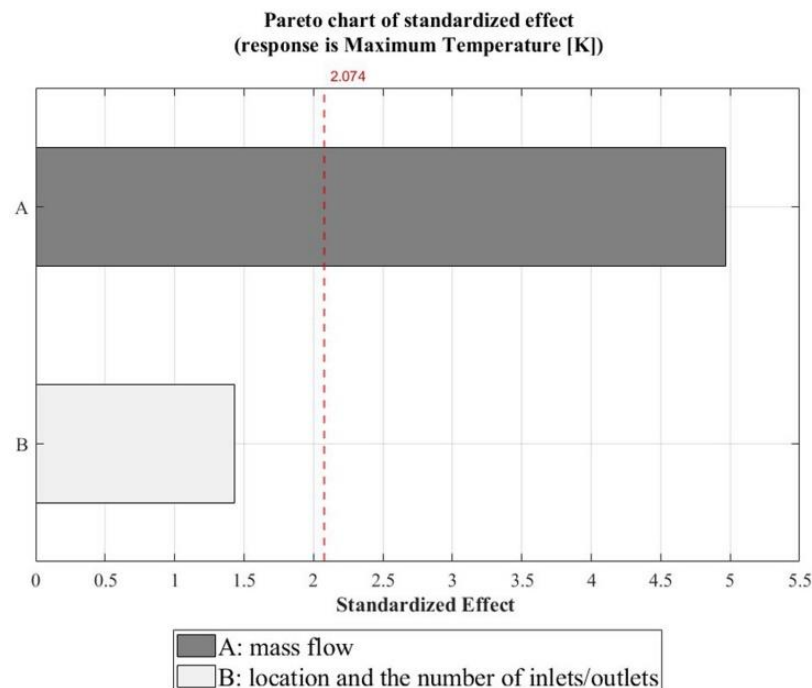


Figure 17. The effects of mass flow change, location, and number of inlets/outlets on maximum temperature.

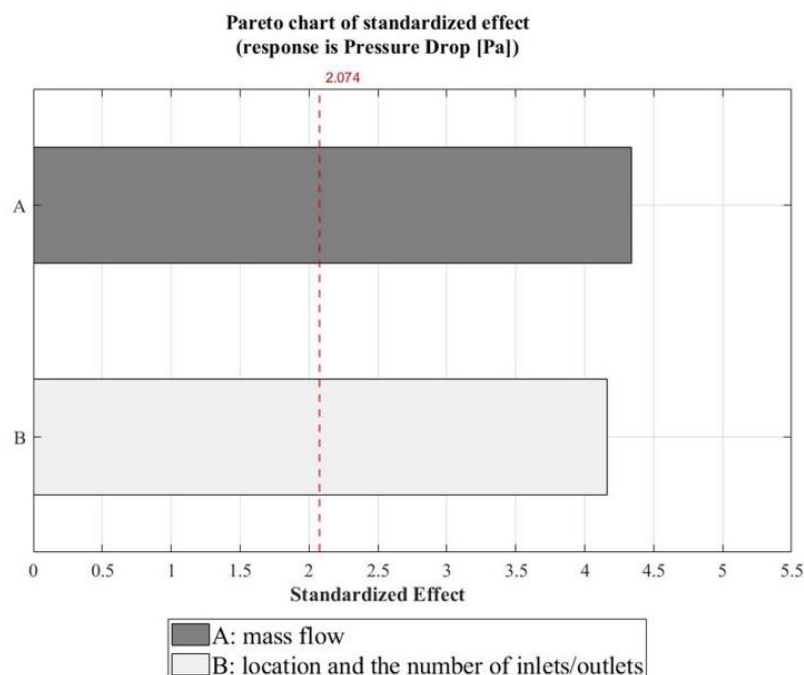


Figure 18. The effects of mass flow change, location, and number of inlets/outlets on pressure drop.

5. Conclusions

In this study, the effects of housing design factors on the maximum temperature of PMSM and the pressure drop of the water jacket were statistically analyzed using the design of experiment (DOE) method. The losses occurring in the maximum operating state of PMSM were calculated using electromagnetic FE analysis and considered as a heat source. The number of water jacket passes was selected by analyzing the maximum PMSM temperature and pressure drop. Subsequently, a statistical investigation using DOE was performed to assess the influence of the number of water jacket passes, the mass flow rate, and the location, as well as the number of inlets/outlets of the water jacket, on the cooling characteristics of the PMSM.

As the number of water jacket passes increased, the maximum temperature of the PMSM decreased, and the pressure drop increased. This is because the heat exchange area of the water jacket increased. After six passes, there was almost no change in the maximum PMSM temperature, and the pressure drop increased exponentially. Therefore, it was found that six passes of the water jacket led to the best cooling performance. As the mass flow rate increased, as is the case with the number of water jacket passes, the maximum temperature of the PMSM decreased, and the pressure drop between the inlet and outlet increased. The maximum PMSM temperature decrease was within 0.8% above flow rates of 0.02547 kg/s, and the pressure drop increased exponentially. Thus, the mass flow rate of 0.02547 kg/s can be considered the optimum condition. In addition, the maximum temperature and pressure drop in PMSM were analyzed according to the location and number of inlets/outlets of the water jacket. As a result of this analysis, it was found that the water jacket with one inlet and two outlets, Model B, had the best cooling performance for reducing the maximum PMSM temperature.

The effects of each design variable on the PMSM cooling performance were investigated using DOE. The results of this study reveal that the mass flow rate is the most critical design factor influencing the PMSM cooling performance. In addition, it was found that the mass flow rate, location, and number of inlets/outlets of the water jacket are important design factors for pressure drop. These findings can be utilized to enhance the cooling performance of the PMSM by incorporating them into the design of cooling devices.

Author Contributions: Conceptualization, H.C., K.J. and C.-W.K.; methodology, K.J., J.-J.L., K.-D.L. and C.-W.K.; software, K.J. and H.C.; validation, K.J. and C.-W.K.; formal analysis, K.J. and M.P.; investigation, K.J. and H.C.; resources, K.J.; data curation, K.J.; writing—original draft preparation, K.J.; writing—review and editing, K.J., J.P., J.-J.L., K.-D.L. and C.-W.K.; visualization, K.J.; supervision, C.-W.K., J.-J.L. and K.-D.L.; project administration, C.-W.K.; funding acquisition, C.-W.K. All authors have read and agreed to the published version of the manuscript.

Funding: This paper was supported by the Technology Innovation Program (20012518) funded By the Ministry of Trade, Industry, and Energy (MOTIE, Korea) and the Konkuk University Researcher Fund in 2021.

Data Availability Statement: Not applicable.

Conflicts of Interest: The authors declare no conflict of interest.

Nomenclature

B_{max}	Maximum magnetic flux density (T)
f	Power supply frequency (Hz)
J	Current density (A/m^2)
k	Electronic conductivity (S/m)
K_h	Hysteresis constant
n	Experimental constant
P_{copper}	Copper loss density (W/m^3)
P_e	Eddy-current loss density (W/m^3)
P_h	Hysteresis loss density (W/m^3)
P_{iron}	Iron loss density (W/m^3)
t	Thickness of the conductor (m)
ρ_{cu}	Specific resistance of the winding

References

1. Borisavljevic, A.; Polinder, H.; Ferreira, J.A. On the Speed Limits of Permanent-Magnet Machines. *IEEE Trans. Ind. Electron.* **2010**, *57*, 220–227.
2. Aldo, B.; Enrico, C.; Marco, C.; Silvio, V. Stator-Winding Thermal Models for Short-Time Thermal Transients Definition and Validation. *IEEE Trans. Ind. Electron.* **2016**, *63*, 2713–2721.
3. Kim, K.C.; Kim, K.S.; Kim, H.J.; Lee, J. Demagnetization analysis of permanent magnets according to rotor types of interior permanent magnet synchronous motor. *IEEE Trans. Magn.* **2009**, *45*, 2799–2802.
4. Jiang, W.; Jahns, T.M. Coupled Electromagnetic–Thermal Analysis of Electric Machines Including Transient Operation Based on Finite-Element Techniques. *IEEE Trans. Ind. Appl.* **2015**, *51*, 1880–1889. [[CrossRef](#)]
5. Aldo, B.; Enrico, C.; Marco, C.; Mircea, P.; Dave, S.; Silvio, V. Equivalent thermal conductivity determination of winding insulation system by fast experimental approach. In Proceedings of the 2015 IEEE International Conference on Electric Machines and Drives (IEMDC), Coeur d’Alene, ID, USA, 10–13 May 2015.
6. Li, W.; Cao, J.; Zhang, X. Electrothermal Analysis of Induction Motor with Compound Cage Rotor Used for PHEV. *IEEE Trans. Ind. Electron.* **2010**, *57*, 660–668.
7. Mi, C.; Gordon, R.S.; Richard, B. Modeling of Iron Losses of Permanent-Magnet Synchronous Motors. *IEEE Trans. Ind. Appl.* **2003**, *39*, 734–742.
8. Inamura, S.; Sakai, T.; Sawa, K. A Temperature Rise Analysis of Switched Reluctance Motor Due to the Core and Copper Loss by FEM. *IEEE Trans. Magn.* **2003**, *39*, 1554–1557. [[CrossRef](#)]
9. Chen, W.; Ju, Y.; Yan, D.; Guo, L.; Geng, Q.; Shi, T. Design and optimization of dual-cycled cooling structure for fully-enclosed permanent magnet motor. *Appl. Therm. Eng.* **2019**, *152*, 338–349. [[CrossRef](#)]
10. Marco, C.; Gloria, G.; Stefano, P.; Enrico, S. Thermal management of a Formula E electric motor Analysis and optimization. *Appl. Therm. Eng.* **2019**, *157*, 113733.
11. Lim, S.H.; Min, S.J.; Hong, J.P. Optimal Rotor Design of IPM Motor for Improving Torque Performance Considering Thermal Demagnetization of Magnet. *IEEE Trans. Magn.* **2015**, *51*, 8202405. [[CrossRef](#)]
12. Rajinder; Sreejeth, M.; Singh, M. Sensitivity Analysis of Induction Motor Performance Variables. In Proceedings of the 2016 IEEE 1st International Conference on Power Electronics, Intelligent Control and Energy Systems, Delhi, India, 4–6 June 2016. [[CrossRef](#)]
13. Zhang, B.; Qu, R.; Fan, X.; Wang, J. Thermal and Mechanical Optimization of Water Jacket of Permanent Magnet Synchronous Machines for EV Application. In Proceedings of the 2015 IEEE International Electric Machines & Drives Conference, Coeur d’Alene, ID, USA, 10–13 May 2015.
14. Ye, Z.N.; Luo, W.D.; Zhang, W.M.; Feng, Z.X. Simulative Analysis of Traction Motor Cooling System Based on CFD. In Proceedings of the 2011 International Conference on Electric Information and Control Engineering, Wuhan, China, 15–17 April 2011.

15. Lee, K.H.; Cha, H.R.; Kim, Y.B. Development of an interior permanent motor through rotor cooling for electric vehicles. *Appl. Therm. Eng.* **2016**, *95*, 348–356. [[CrossRef](#)]
16. Liang, P.; Chai, F.; Shen, K.; Liu, W. Thermal design and optimization of a water-cooling permanent magnet synchronous in-wheel motor. In Proceedings of the 2019 22nd International Conference on Electrical Machines and Systems, Nanchang, China, 20–22 June 2011. [[CrossRef](#)]
17. Altair Flux 2018 User Guide. Available online: <https://2022.help.altair.com> (accessed on 31 May 2023).
18. Shervin, S.S.; Richard, M.; John, W.; Denise, R.; Katherine, S. An Electric Motor Thermal Bus Cooling System for Vehicle Propulsion—Design and Test. *SAE Int. J. Adv. Curr. Prac. Mobil.* **2020**, *2*, 1–8.
19. Montgomery, D.C. *Design and Analysis of Experiments*, 7th ed.; John Wiley & Sons, Inc.: Hoboken, NJ, USA, 2009.
20. PIAO 2019 Help. Available online: http://www.pidotech.com/reference/reference01.php?ptype=view&idx=388&page=1&code=reference01_silver (accessed on 29 April 2023).

Disclaimer/Publisher’s Note: The statements, opinions and data contained in all publications are solely those of the individual author(s) and contributor(s) and not of MDPI and/or the editor(s). MDPI and/or the editor(s) disclaim responsibility for any injury to people or property resulting from any ideas, methods, instructions or products referred to in the content.